Journal of Colloid and Interface Science 555 (2019) 810–817

Contents lists available at ScienceDirect

Journal of Colloid and Interface Science

journal homepage: www.elsevier.com/locate/jcis

Hydrogen bonding and molecular orientations across thin water films on sapphire

Jean-François Boily [a,*], Li Fu [b,1], Aashish Tuladhar [b], Zhou Lu [c], Benjamin A. Legg [b], Zheming M. Wang [b], Hongfei Wang [d]

[a] Department of Chemistry, Umeå University, SE 907 87, Umeå, Sweden
[b] Physical Sciences Division, Pacific Northwest National Laboratory, Richland, WA 99352, USA
[c] Beijing National Laboratory for Molecular Sciences, CAS Research/Education Center for Excellence in Molecular Sciences, Institute of Chemistry, Chinese Academy of Sciences, Beijing 100190, China
[d] Department of Chemistry and Shanghai Key Laboratory of Molecular Catalysis and Innovative Materials, Fudan University, Shanghai 200438, China

GRAPHICAL ABSTRACT

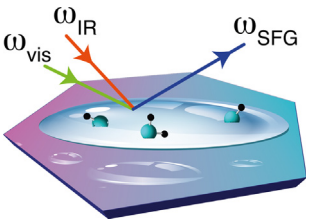

ARTICLE INFO

Article history:
Received 12 July 2019
Revised 7 August 2019
Accepted 8 August 2019
Available online 09 August 2019

Keywords:
Sapphire
Water
Film
Sum frequency generation
Molecular dynamics
Spectroscopy
Hydration
Atmosphere

ABSTRACT

Hypothesis: Water vapor binding to metal oxide surfaces produces thin water films with properties controlled by interactions with surface hydroxo sites. Hydrogen bonding populations vary across films and induce different molecular orientations than at the surface of liquid water. Identifying these differences can open possibilities for tailoring film-mediated catalytic reactions by choice of the supporting metal oxide substrate.
Experiments: The (0001) face of a single sapphire (α-Al_2O_3) sample exposed to water vapor and the surface of liquid water were probed by polarization dependent Sum Frequency Generation-Vibration Spectroscopy (SFG-VS). Molecular dynamics (MD) provided insight into the hydrogen bond populations and molecular orientations across films and liquid water.
Findings: SFG-VS revealed a submonolayer film on sapphire exposed to 43% relative humidity (R.H.), and a multilayer film at 78% R.H. Polarization dependent SFG-VS spectra showed that median tilt angles of free O—H bonds on the top of films are at ~43° from the normal of the (0001) face but at 38° on neat liquid water. These values align with MD simulations, which also show that up to 36% of all O—H bonds on films are free. This offers new means for understanding how interfacial reactions on sapphire-supported water films could contrast with those involving liquid water.

1. Introduction

Metal oxide surfaces exposed to atmospheric water stabilize thin water films of various thickness and degrees of organization (Fig. 1) [1–6]. These films can solubilize gases and ions in highly unique ways, and host reaction of crucial importance to

Abbreviations: GDS, Gibbs dividing surface; HB, hydrogen bond; MD, molecular dynamics; R.H., relative humidity; SFG-VS, sum frequency generation spectroscopy-vibration spectroscopy; XPS, X-ray photoelectron spectroscopy.

* Corresponding author.
E-mail address: jean-francois.boily@umu.se (J.-F. Boily).
[1] Current address: Sanofi-Genzyme, 1 The Mountain Road, Framingham MA 01532, USA.

https://doi.org/10.1016/j.jcis.2019.08.028
0021-9797/

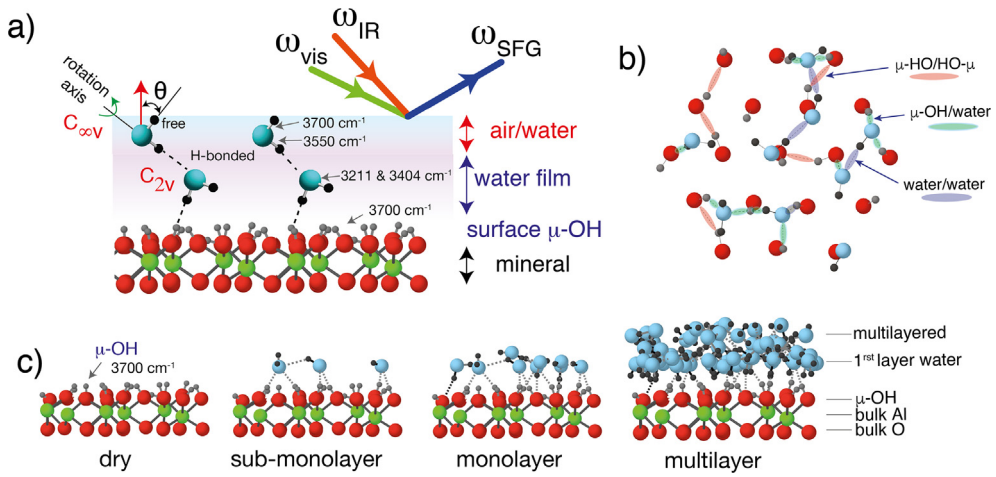

Fig. 1. Schematic representation of water films on the (0001) basal face of sapphire (α -Al_2O_3). (a) Idealized hydrogen bonding environment in a multilayered film, showing angle (θ) of the topmost water molecules of the water/air interface, optical geometry by SFG-VS, and key band assignments. These topmost water molecules are of C_{∞} symmetry (free OH at 3700 cm^{-1}), unlike the tetrahedrally-coordinated molecules below the surface (hydrogen bonded OH at 3211 and 3404 cm^{-1}). (b) Basal face view, here extracted from a snapshot of a Molecular Dynamics simulation with 30 $H_2O{\cdot}nm^{-2}$, showing the spatial distribution and (color-coded) hydrogen bonding patterns involving the first layer water molecules. (c) Schematic representation of sideview of the (0001) basal face at different water loadings.

environmental and technological processes where solids are exposed to atmospheric water vapor. Advancing knowledge on the nature of water molecules in these films is essential for the scientific community's pursuit of understanding processes relevant to fields as varied as vadose zone geochemistry, atmospheric cloud chemistry, (photo)catalysis, microfluidics, rheology and tribology.

Water films develop when water vapor (i) binds directly onto metal oxide surface sites, forming the first few layer waters of films (*adsorption* regime), and (ii) grow further via water-water interactions (*condensation* regime) [7]. Moving current-day boundaries in this area requires combined knowledge from the metal oxide/water [8–17] and water/air literature [18–27], two fields that have received far more attention than material-supported water films. Knowledge of hydrogen bond populations and of water orientation across supported water films remains, as such, increasingly needed as new possibilities are emerging for understanding processes across and on these films (*e.g.* gas dissolution, photosensitive reactions, monolayer assembly). One notable example of where such knowledge is needed includes a recent study showing how water film thickness tailors CO oxidation on gold [28].

Although experimental work involving oxide nanoparticles [29,30] can be advantageous for addressing water binding phenomena, interparticle capillary condensation can add complexity to the host of reactions under study. Single oriented surfaces minimize these contributions and create possibilities for following film growth mechanisms. Additionally, they offer an ideal setting for directly probing the water/air component of water films. They consequently provide possibilities for advancing knowledge on the chemistry of the topmost water molecules responsible for film growth and gas exchange reactions.

In this study, Sum Frequency Generation Vibrational Spectroscopy (SFG-VS) and molecular modeling were used to explore water films formed by the adsorption and condensation of water vapor on the basal (0001) face (C-plane) of sapphire (α-Al_2O_3) [18,19,22,25,31–34]. The hydroxylated form of this face is of great significance to earth sciences and technology as it exposes free and weakly-hydrogen bonded hydroxyl groups [35–37] responsible for the attachment of water (Fig. 1) and a score of solvent-mediated catalytic reactions.

This SFG-VS work provides insight into the dominant hydroxyl functional groups outcropping the (0001) face, and of the water films formed by adsorption and condensation of water vapor. MD simulations provide insight into hydrogen bond populations formed in and across the films, especially to contrast with populations formed in bulk liquid water. These properties will also be compared to those of the water/air interfacial region of neat water, and will account for a recently-proposed [38] modification of a geometric definition of hydrogen bonds in this region. A theory-supported analysis of the polarization dependence of SFG-VS spectra will demonstrate how the orientation of free O—H bonds in the top portions of both sapphire-supported water films differs from that of the surface of liquid water. This suggestion promotes further polarization dependent SFG-VS as a means for tracking the orientation of the topmost water molecules during (*e.g.* gas exchange, (photo)catalysis) reactions. This should be especially important for future studies aimed at testing hypotheses linking the orientation of these topmost water molecules to mechanisms and energetics of interfacial reactions.

2. Materials and methods

2.1. Synthetic sapphire

Synthetic sapphire samples were purchased from SurfaceNet GmbH (Rheine, Germany). The samples were grown with the Kyropoulos crystal growth method [39], cut as 3 × 3 × 3 mm cubes, and mechanically and chemically polished along the (0001) face. The orientation of the face was confirmed by high resolution digital Laue (Photonic Science). X-ray photoelectron spectroscopy (XPS; Kratos Axis Ultra) confirmed that the sample surfaces was terminated by Al_2O_3 and surface hydroxo groups, although with a slight (2.28 atomic %) contamination by fluoride resulting from the sample preparation process (Table S1, Fig. S1). Organic contaminants (Table S1) were removed prior all SFG experiments by ozonation (PSD Pro Series). SFG measurements (Section 2.2) confirmed the absence of organics during water vapor binding experiments, seen through the absence of intensities in the C—H stretching region. Finally, XPS (Table S1, Fig. S1) also showed that prior exposure to atmospheric CO_2 did not produce (bi)carbonate complexes resilient to degassing. This falls in line with previous findings from our group showing weak CO_2 interactions with μ-OH groups [40].

High-resolution atomic force microscopy images of the cleaned surfaces were obtained with a Cypher ES (Oxford Instruments),

operated in amplitude-modulated mode using an NCL-W probe (Nanoworld, nominal tip radius = 8 nm, k = 16 N/m). Images (Fig. S2) show step-edges spaced with a height on the order of 2.0–2.5 Å, which is consistent with the 2.16 Å spacing between the Al layers of sapphire on the (0001) face. The average step-edge spacing of 27 ± 3 nm indicates a cut that is locally within 0.6° of parallel to the (0001) face.

2.2. Sum frequency generation – vibration spectroscopy

SFG-VS measurements were collected on a clean sample placed in an air-tight N_2(g) flow-through cell (Praying Mantis™, Harrick Scientific Products, Inc.) equipped with CaF_2 windows. The windows of the cell enabled an optical path for the fixed visible beam (532.1 nm) at an incident angle $\beta_1 = 45 \pm 1°$, and of a tunable (1000–4000 cm^{-1}) infrared beam at $\beta_2 = 55 \pm 1°$. The SFG-VS signal was detected in reflection geometry. This geometry was chosen to enhance the relatively weak signal of the top-most water molecules of the water/air interface.

The headspace of an air-tight flow-through cell was continuously flushed upon delivery of N_2(g) at 0, 43 and 78% relative humidity (R.H.) using clean stainless-steel tubing. Atmospheres of 43 and 78% R.H. were generated by bubbling dry N_2(g) in $CaCl_2$ solutions at predetermined concentrations [41]. The partial pressures of these equilibrated gases were determined by non-dispersible infrared spectrometry (LI-7000, Licor, Inc). Prior SFG-VS analysis, the sample was first exposed to dry N_2(g) to remove CO_2 and possibly adventitious atmospheric organic volatiles from the surface for a few hours. SFG-VS spectra were thereafter exposed to further to 0% R.H. or to 43 or 78% R.H., and equilibrated further for a 30 min period prior measurements. In a second set of experiments, SFG-VS spectra of the neat water/air interface were collected for the surface of doubly distilled deionized water exposed to an atmosphere of N_2(g).

The visible beam used for SFG-VS was typically less than 260 μJ, while the energy of the tunable IR beam 175 μJ in the 2800–4000 cm^{-1} range. These energies were chosen after a number of preliminary experiments at higher values showed that they did not damage the sample and did not evaporate thin water films. The latter was confirmed further in preliminary experiments showing that SFG spectra did not change over the course of ~1 h. Measurements were performed at a frequency interval of 5 cm^{-1}, and the recorded intensity at each frequency was the average of 150 laser pulses under *ssp* and 300 pulses under *ppp* polarization. These notations (*ssp*, *ppp*) refer to the polarization angles of (i) the electric field for the directional SF signal, (ii) the visible beam, and (iii) the IR beam, respectively [42].

All SFG-VS spectra were normalized to the non-resonant SFG-VS of a Z-cut quartz crystal surface in its *x*-direction [43–45], and were fitted using a Lorentzian shape function, as in previous SFG-VS work [42], with:

$$I_{SFG-VS} \propto \left| \chi^{(2)}_{NR} + \sum_k \frac{A_k}{\omega_{IR} - \omega_k - i\Gamma_k} \right|^2 \quad (1)$$

In this function, $\chi^{(2)}_{NR}$ is the nonresonant contribution to the discrete vibrational modes and the right-hand term the resonant contributions. The latter are expressed as a function of frequency ω_{IR} for the sum of k bands of central frequency ω_k, transition line width (full width at half maximum) Γ_k, and amplitude A_k.

An analysis of the orientation of the free OH group of the top-most layer of the sapphire and water film surfaces (Fig. 1) was estimated with [26,42]:

$$D = \frac{\langle cos\theta \rangle}{\langle cos^3\theta \rangle} = \frac{d_{ssp} \times c_{ssp} - d_{ppp} \times R}{d_{ssp} - d_{ppp} \times R} \quad (2)$$

This equation relates the orientational parameter $D = \langle \cos\theta \rangle / \langle \cos^3\theta \rangle$ to the ratio of the intensities of the bands at 3700 cm^{-1} under *ssp* and *ppp* polarization (R). The angle (θ) is between the vector of the free O—H bond and the axis normal to the (0001) face. The strength factor (d_{ssp}, d_{ppp}) and general orientation (c_{ssp}) parameters for the optical geometry of this study are taken from Gan et al. [25]. We note that our approach is at odds with the views [38,46] for an exponential distribution of free OH bond angle distributions, and refer to Gan et al. [47] and Sun et al. [48] for recent thoughts on this matter.

2.3. Molecular modeling

Classical Molecular Dynamics (MD) simulations were performed to provide clues on the plausible configurations of thin water films on the (0001) face of sapphire. Although this approach cannot account for proton exchange reactions between water and the terminating μ-OH groups, these reactions are expected to be negligible considering (*i*) the absence of counterions enabling charge development, and (*ii*) that the pH = 7 of the film is close to the point-of-zero-charge/isoelectric point (4–7) of this face [49,50]. The pH the simulated film is thereby 7 and the surface charge is neutral, which are representative values of the surfaces studied experimentally. The absence of charge generation, and of significant levels of proton transfer – also confirmed in recent *ab initio* MD simulations of this [51] and analogous basal faces [52] – thus motivates further the use of classical MD for this work. This approach has for added benefit for enabling simulations of larger systems and long simulation times.

The simulation cell was a 3.25 nm × 3.88 nm × 3.09 nm (*xyz*) slab ($Al_{1792}O_{2496}OH_{394}$) exposing two (0001) faces perpendicular to the *z*-direction contacted in a ~5 nm thick void containing various quantities of water molecules. The slab was cut from a slightly thicker 3D periodic cell generated from the crystallographic structure [53] of sapphire, and pre-equilibrated by MD. Each (0001) face was terminated by 192 μ-OH (*i.e.* Al_2-OH) groups to complete the coordination environment of surface Al atoms, and to achieve charge neutrality in the entire simulation cell.

Simulations were carried out using classical MD using Gromacs 2018 [54]. Sapphire was simulated using the CLAYFF [55] force field, using the newly adapted parameters [52] for aluminum (hydr)oxides and its surface OH groups of the basal face, and water was simulated with the SPC/Fw model [56], a flexible variant of the rigid SPC model [57]. The O—H bond strengths of the surface μ-OH group of sapphire was set to harmonic potential constant 460530 $kJ{\cdot}mol^{-1}{\cdot}nm^{-2}$ to match the experimental frequency (~3700 cm^{-1}) detected in this work. In an additional simulation, a 4.0 × 4.0 × 4.0 nm box of 2180 water molecules contacted with an empty box of the same dimension was used study the neat water/air interface.

Both sapphire/water and neat water systems were simulated using a NVT (constant number of particles, constant volume and constant temperature) ensemble. A time step of 1.0 fs was used with the Verlet algorithm [58] to integrate the equations of motions for all the atoms in the system, which were projected to infinity using a periodic boundary condition. The temperature of the system (300 K) was coupled to the Nosé-Hoover [59] velocity-rescale thermostat with a 0.1 ps relaxation time. The SETTLE algorithm [60] was used to treat the geometry of water and the LINCS algorithm [61] were used to treat the O—H bonds of all hydroxyls. Position constraints were not used in any case. A 0.8 nm cut-off was used for van der Waals interactions, and the particle mesh Ewald method[25, 26] was used to treat long-range electrostatic interactions. Simulation cells were first energy-minimized using a steepest descent algorithm, typically in less

than 10^4 steps. The minimized structures were then equilibrated using classical MD for 10^7 steps (5 ns). Additional 20 ns simulations were then generated for production runs to monitor atomic positions and energies, and sampled every 1000 steps.

Trajectory analyzes were made using Gromacs 2018 and customized codes written for this study. Hydrogen bond (HB) populations were analyzed for (*i*) the entire film as function of water loading, and (*ii*) across single films. Hydrogen bonds were those with donor (D)-acceptor (A) bond of $R \leq 0.35$ nm and H-D-A angles of $\beta \leq 30°$, as in Luzar and Chandler [62] and based on previous work [63,64]. We also consider the more recently proposed possibility of $\beta \leq 50°$ as a means to exclude weakly hydrogen-bonded water molecules of the water/air interface [38]. These analyses identified free OH groups at every time step, and permitted calculations of the orientation of every free OH with respect to the normal of the film surfaces (θ, as in Fig. 1).

3. Results and discussions

3.1. SFG-VS

SFG-VS measurements (Fig. 2) of the dry (0 R.H.) sapphire surface under *ssp* polarization detected terminating OH functional groups [35,51,64–67] through a single, yet broad, band centered at 3700 cm^{-1}. This is consistent with previous SFG-VS work [35,36,69] on the hydroxylated (0001) face of α-Al_2O_3 and, despite possible variations in properties (roughness, co-existence of hydrophobic nanopore [37]) that can arise from differences in sample preparation, the band is predominantly generated by μ-OH groups exposing the hydroxylated (0001) sapphire surface. The band is fitted with a single Lorentzian component (Eq. (1)) with a transition line width of $\Gamma = 92$ cm^{-1}, suggesting a various bond strengths for these OH groups. Deconvolution of this region with two bands did not provide a statistically significant improvement in the goodness of fitting. The substantially lower intensities of the spectrum for *ppp* polarization also suggest that the OH groups are generally oriented towards the normal of the surface, as previously suggested [35]. Using the theory of Wang et al. [25,26,42] (Eq. (2); Fig. S3), the intensity ratios of the 3700 cm^{-1} bands under *ssp* and *ppp* suggest an average O—H bond orientation of $\theta = 38°$ from the normal of the surface. By comparison, Zhang et al. [35] reported $\theta = 26°$ on a different sample, with likely a different preparation history.

Exposing the sample to 43% R.H. increased the intensities of 3300–3700 cm^{-1} region (Fig. 2). Consistent with related work on nanoparticles from our group [29,30,70,71], the intensification of this region is explained by (i) a weakening of the O—H stretch of μ–OH caused by hydrogen bonding with water molecules, and (ii) overlapping contributions from these adsorbed water molecules The absence spectral features of the topmost region of liquid water (Fig. 2) [30,71], suggests that the surface must be populated by less than the equivalent of about two monolayers of water (*e.g.* Fig. 1c).

Exposing the sapphire surface to 78% R.H. produced two new bands at 3211 and 3404 cm^{-1}, consistent with the appearance of a liquid-like water film [30,71], and not those of hexagonal ice [72]. These liquid-like water bands are even comparable to those of liquid water on sapphire [17]. In this case, the 3700 cm^{-1} band of the *ssp* spectrum is no longer shifted to lower values, as in 43% R.H., but has nearly doubled in intensity and narrowed from $\Gamma = 49$ cm^{-1} to 40 cm^{-1}.

We explain the intensification and narrowing of the ~3700 cm^{-1} band with the appearance free OH bonds from water molecules of the topmost portion of the films (Fig. 1). Comparison with spectra of the neat water/air interface (Fig. 2a) [24 25–27] reveals a striking similarity with an intense ~3700 cm^{-1} and narrower ($\Gamma = 13$ cm^{-1}) band under *ssp* polarization. The appearance of this band was also used by Miranda et al. [72] as an indicator for a multilayer water film on mica, as a monolayer-like film would not expose free OH groups akin to those of the neat water/air interface. We also note that the ~3700 cm^{-1} band remained broader in the sapphire-supported films than in neat water because (*i*) larger ranges of bond strengths are likely to be adapted by these topmost water molecules, (*ii*) sub-populations of μ–OH groups can be decoupled from the HB network and develop free O—H bonds (*cf.* shoulder at 3824 cm^{-1} in Fig. 2a; *ab initio* MD studies of Melani et al. [65], Ma et al. [12]), and (*iii*) free OH stretches of water could even persist within the film (*cf.* Boulesbaa and Borguet [69]).

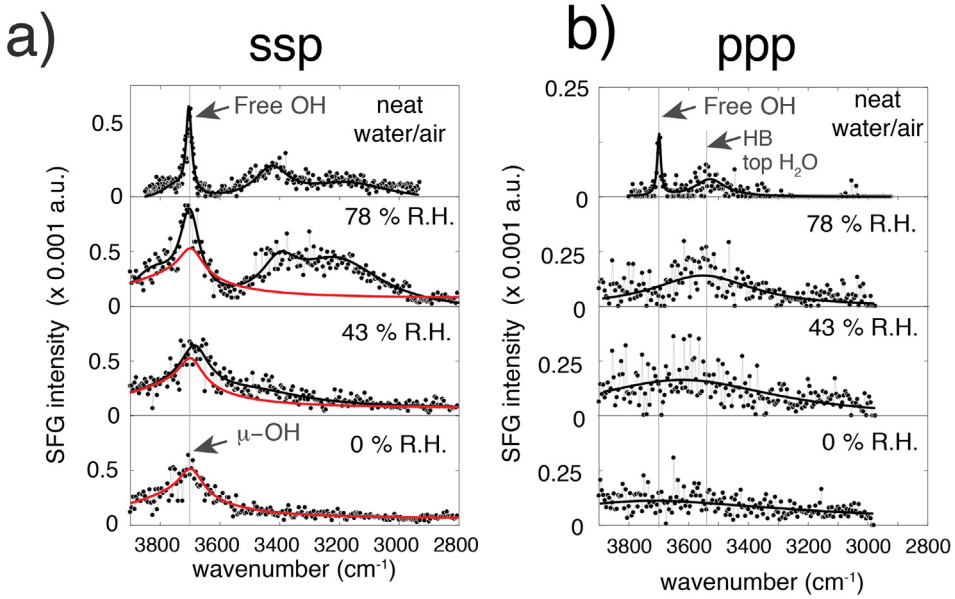

Fig. 2. SFG-VS data of the neat water/air interface, and of a single (0001) face of sapphire exposed to N_2(g) and water vapor at 25 °C. Spectral data are for (a) *ssp* and (b) *ppp* polarization, and fitted using a linear combination of Lorentzian components (full lines) with Eq. (1). Red lines in (a) are of the dry (0001) face at 0% R.H, shown for comparison. (For interpretation of the references to color in this figure legend, the reader is referred to the web version of this article.)

Contributions of topmost water molecules to the ~3700 cm^{-1} band region are confirmed further in the spectra under *ppp* polarization (Fig. 2b), a finding that contrasts with previous *ppp* SFG-VS spectra by Zhou et al. [73] who reported very little water binding on this face. The intensification in the SFG in the ~3550 cm^{-1} region of the *ppp* spectrum is strongly comparable to that of the neat water/air interface [24–27], and is likely generated by a donating HB group from the topmost to underlying water molecules (Fig. 1a).

Using the theory of Wang et al. [25,26,42] (Eq. (2)), we used the intensity ratios of the 3700 cm^{-1} bands under *ssp* and *ppp* estimate the average tilt of the free O—H bond at the surface of the water films (*cf.* Fig. S3 for polarization dependence of the SFG-VS intensity). The larger intensity ratio in the film at 78% R.H. than on neat water point to an increase in tilt angle to $\theta = 43°$. This contrasts with $\theta = 38°$ (35° in a previous work [26]) at the neat water/air interface. This result thus already hints to the possibility that the internal structure/hydrogen bonding network of the thin water film could be responsible for orienting the free OH bond closer towards the (0001) face than on neat water. This analysis for the 43% R.H. data retrieves an average tilt angle of 35°, that however results from contributions of *both* unreacted μ-OH groups ($\theta = 38°$) and the thinner water film.

3.2. Molecular modeling

MD simulations of the (0001) face added further insight into plausible molecular configurations adopted by water films of various loadings. The most relevant simulations used to follow water film growth are those from sub-monolayer to multilayer films (Fig. 1c) with transitioning towards those of liquid water above 5–6 layers (Fig. 3). This transition can first be appreciated by the increase in the thickness (2δ) of the water/air interfacial region (Fig. 3a), as expressed through the function:

$$p(z) = a\left(1 - \tanh\left(-\frac{z - z_G}{\delta}\right)\right) \quad (3)$$

In this equation, the Gibbs Dividing Surface (GDS) is located at z_G where a is the half of the thin water film density. This analysis showed that 2 δ increased from a single water monolayer (~2.6 Å) at 15 $H_2O{\cdot}nm^{-2}$ to values comparable to those of the neat water/air interface (~3.4 Å; *cf.* dashed line in Fig. 2a) [23,74] in multilayered films (~3.8 Å in 30 $H_2O{\cdot}nm^{-2}$).

Simulations (Fig. 3b) show that up to ~70% of μ –OH groups form hydrogen bonds (HB) with adjacent μ –OH groups (~30%) and water molecules (~40%) (*cf.* Fig. S4 for a breakdown of populations). Donating (μ –OH···OH_2) and accepting (μ –OH···H_2O) interactions do not, however, alter the pre-existing HB populations between μ –OH groups buried ~0.3 nm below the first water layer. These results thus fall in line with previous simulation studies [12], and with our SFG results revealing the co-existence of free μ –OH groups in water films. It also infers the presence of HB of various strength, which could be consistent with the relatively large transition line with of the 3700 cm^{-1} band.

Water-water interactions involved ~2.8 HB/H_2O in a single monolayer film to values of converging towards those of liquid water (~3.4 HB/H_2O) at greater loadings equivalent to at least 5–6 layers (Fig. 3b). Populations of the same forms of interactions *across* films (Fig. 4) however underscored the important heterogeneity of these water films, and thereby how they depart from those in liquid water. Here focusing the discussion on a film with 30 $H_2O{\cdot}nm^{-2}$ (Fig. 4), and a representative multilayered water film (Fig. 1c), simulations show that the near surface region controlled by interactions with μ –OH ($\sim z_G - 0.6$ nm) allows mostly 1–2 HB between neighboring water molecules. Second layer molecules ($\sim z_G - 0.3$ nm) adopt, on other hand, the highest levels of HB, and thereby constitute the most 'liquid-like' portion of the film (*cf.* HB population of liquid water in Fig. 4c). Still, an average of 26% of these molecules have free OH bonds, compared to only 18% in bulk liquid water. Additionally, these populations are enriched further towards the interfacial region ($z_G - \delta \rightarrow z_G + \delta$), with an average 36% of free OH bond in the film and 33% in neat water. Repeated HB analyses using a cutoff of $\beta \leq 50°$ for the H-D-A bond angle, as advocated in recent studies [38,46], decreased populations of free OH bonds to 23% in the film and to 25% on neat water.

Differences in the free OH bond populations of water in the films and liquid water are manifested further in the average orientations (θ) of these bonds (Fig. 5; Table 1). Tilt angles adopt normal-type distributions, and not the exponential distributions reported in a recent study [46] as recently expressed by Gan et al. [47]. This is consistent with SFG-VS work under multiple geometries confirming that the orientation distribution should be narrow [25,26,75]. Angles also shift from water molecules pointing towards the sapphire surface in the deep portion of the films

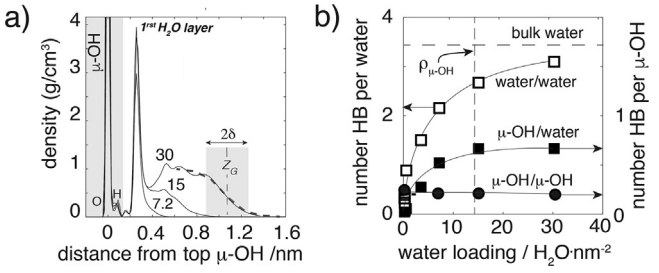

Fig. 3. MD simulations of water films on sapphire. (a) Water density profiles at 0.6 to 30 $H_2O{\cdot}nm^{-2}$, including the density profile of μ –OH groups (shaded portion on the left-hand side). The Gibbs Dividing Surface (GDS; Eq. (3)) centered at z_G nm from the top μ–OH group and the thickness of the interface (2 δ) are shown for 30 $H_2O{\cdot}nm^{-2}$. A portion of the density profile centered around the GDS of a neat water/air interface is shown in dashed grey for comparison. The *head* of the water/air interface is at $z_G - \delta$ while the *tail* at $z_G + \delta$. (b) Hydrogen bond (HB) populations for three forms of interactions for the entire water film (*cf.* Fig. 1). HB population for water/water interactions in bulk liquid water at 25 °C (horizontal dashed line) and the crystallographic density of μ-OH groups ($\rho_{\text{-OH}}$; vertical dashed line) are also shown. See Fig. S6 for full breakdown of HB interactions.

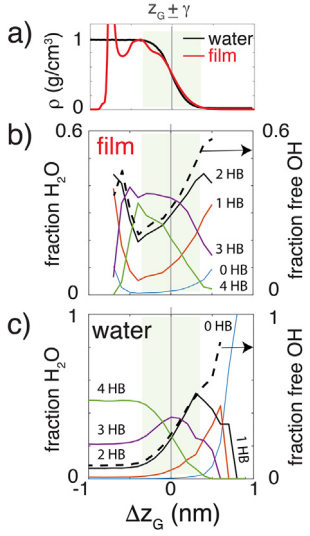

Fig. 4. MD simulations of water films on sapphire. (a) A portion of water density profiles of Fig. 3a, here shown for the near interfacial region ($z_G \pm \delta$) of a film with 30 $H_2O{\cdot}nm^{-2}$ and for neat water. (b and c) Fraction of water molecules involved in 0–4 HB (full lines; left ordinate axis) and fraction of free OH bonds (dashed line; right ordinate axis) *across* (b) a film at 30 $H_2O{\cdot}nm^{-2}$ and (c) neat water.

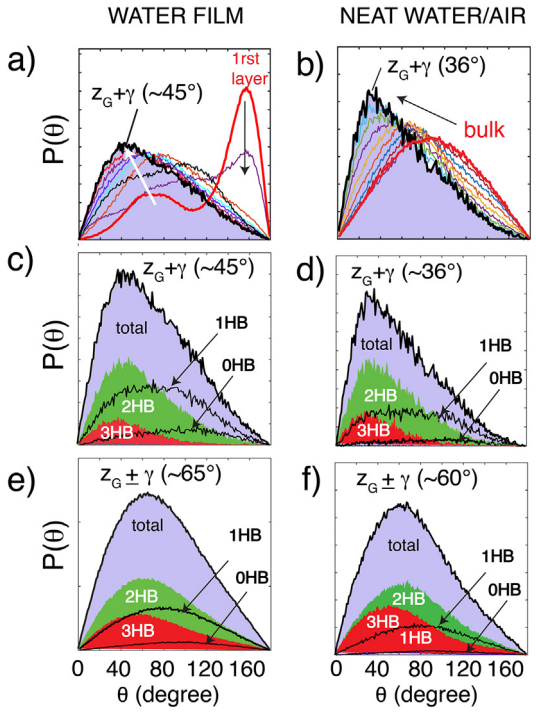

Fig. 5. MD-derived orientation of interfacial water molecules (θ, *cf.* Fig. 1a) in sapphire-supported water films (a, c and e) and on neat water (b, d and f). A hydrogen bond is here defined as in Luzar and Chandler [62], and yields comparable angle distribution than using a more recent definition [38,46] using a H-D-A angle of $\beta \leq 50°$ (*cf.* Fig. S5). Distribution at (a and b) the tail of the interfacial region ($z_G + \delta$), and within the interfacial region ($z_G \pm \delta$), with angles specified at $P(\theta)_{max}$ in both cases (arrows in (a) and (b) show transition from bulk to surface). Angle distributions are broken down in contributions from water with 0–3HB, and show that 2HB and 3HB interfacial waters are predominantly responsible for the water distributions. The analyzes shown in Fig. S6 confirm that interfacial water are both donors and acceptors.

Table 1
Centers of tilt angle (θ) distributions (Fig. 5).

	Film (30 H_2O/nm^2)		Neat water	
	$\beta \leq 30°$	$\beta \leq 50°$	$\beta \leq 30°$	$\beta \leq 50°$
$z_G + \delta$	45°	43°	36°	33°
$z_G \pm \delta$	66°	54°	64°	59°
entire film	72° & 154°	73° & 156°		

($\theta \sim 156°$), to broader distributions centered at $\theta \sim 45°$ (43° when $\beta \leq 50°$) at the *tail* of the interfacial region ($z_G + \delta$). By comparison, angle distributions in water conform to a sin(θ) function for homogeneously distribution free OH bonds in the bulk, and shift to $\theta \sim 36°$ (33° when $\beta \leq 50°$) at the water/air interface. These two set values therefore highly align with our polarization dependence analysis (Eq. (2)), however with the notable exception that they hold for the very top most portion of interfacial water molecules. Taking the values for the deeper portions of interfacial region ($z_G - \delta$) yields a broader distribution centered at $\theta \sim 66°$ (54° when $\beta \leq 50°$) in water films, and $\beta \sim 64°$ (59° when $\beta \leq 50°$) on neat water. These values are consistent with simulated values [38,46,76] for neat water that also consider the entirety of the interfacial region, and incidentally include greater contributions from the more random bulk.

These efforts consequently show how an adequate selection of the portion of the interfacial region is key for comparing SFG-VS and simulations. In the light the data of this study and of previous work [25,26,75], we assert that the strong sensitivity of the *ppp* intensity to experimental optical geometry can only result from a fairly narrow orientational distribution of free OH bonds. The tilt angle of the free OH bond of water is centered at 43° for films on sapphire, and at 38° on neat water. MD simulations suggest that these tilt angles pertain only to the topmost region of the interface.

4. Conclusions

This work provides evidence that water films on sapphire develop considerably different solvation environments than at the surface and bulk of liquid water. This was seen in the orientation of the topmost region of the water surfaces — with a tilt angle centered at 43° for films on sapphire and 38° on neat water — down to the deeper portions of the films where water molecules are hydrogen bonded to μ–OH groups. It was also manifested in the greater proportions of free OH bonds of films, which host contrasting hydration environments for solutes across the sapphire/water/air interface. These findings validate the working hypothesis that film interactions with hydroxo groups of metal oxide surfaces impact hydrogen bonding populations and molecular orientations.

This work also demonstrates the strength of our theory-based analysis [25,26,42] of polarization dependent SFG-VS for tracking the orientation of topmost water molecules on material-supported water films. It thus expands previous the applicability of the approach from liquid water surfaces only [25,26,42], and shows that comparison between experiment and theory can be achieved by considering the very top most portion of the film surface ($z_G + \delta$). This not only opens new possibilities for re-examining previous studies on related systems [36,77,78] but also emboldens new efforts testing hypotheses that link the orientation of topmost water molecules to mechanisms and energetics of interfacial reactions. Future studies considering variations in metal oxide composition and structure could thus offer promising avenues for evaluating if these contrasting properties do impact interfacial reaction pathways. We foresee that work focused on gas (*e.g.* CO_2, SO_X, NO_X, O_2) dissolution, chiral selection, and monolayer self-assembly could help open these avenues. These types of studies should be especially beneficial to natural sciences and to film engineering.

Acknowledgements

This work was supported by the Swedish research council, Sweden to J.-F.B. (VR 2016-03808), the Carl-Tryggers Foundations, Sweden and the Kempe Foundations, Sweden. A portion of this research was conducted using the resources of High Performance Computing Centre North (HPC2N) at Umeå University. All SFG-VS work was performed using EMSL (Ringgold ID 130367), a DOE Office of Science User Facility sponsored by the Office of Biological and Environmental Research, User Project # 49764 to J.-F.B. A.T. also acknowledges the support provided by the US Department of Energy (DOE), USA, Office of Basic Energy Sciences, Division of Materials Science and Engineering at Pacific Northwest National Laboratory (PNNL). A. Shchukarev (Umeå University) is thanked for XPS analyses.

Appendix A. Supplementary material

Supplementary Material file contains AFM imaging data, theoretical polarization dependence on the SFG-VS intensities, as well as detailed analyses of MD simulations. Supplementary data to this article can be found online at https://doi.org/10.1016/j.jcis.2019.08.028.

References

[1] D.E. Moore, D.A. Lockner, Crystallographic controls on the frictional behavior of dry and water-saturated sheet structure minerals, J. Geophys. Res.: Solid Earth 109 (B3) (2004) B03401.
[2] D. Argyris, N.R. Tummala, A. Striolo, D.R. Cole, Molecular structure and dynamics in thin water films at the silica and graphite surfaces, J. Phys. Chem. C 112 (35) (2008) 13587–13599.
[3] G.E. Ewing, Ambient thin film water on insulator surfaces, Chem. Rev. 106 (4) (2006) 1511–1526.
[4] G.A. Kimmel, M. Baer, N.G. Petrik, J. VandeVondele, R. Rousseau, C.J. Mundy, Polarization- and azimuth-resolved infrared spectroscopy of water on TiO_2(110): anisotropy and the hydrogen-bonding network, J. Phys. Chem. Lett. 3 (6) (2012) 778–784.
[5] N.G. Petrik, G.A. Kimmel, Hydrogen bonding, H-D exchange, and molecular mobility in thin water films on TiO_2(110), Phys. Rev. Lett. 99 (19) (2007).
[6] J.C.C. Santos, F.R. Negreiros, L.S. Pedroza, G.M. Dalpian, P.B. Miranda, Interaction of water with the gypsum (010) surface: structure and dynamics from nonlinear vibrational spectroscopy and Ab initio molecular dynamics, J. Am. Chem. Soc. 140 (49) (2018) 17141–17152.
[7] D.D. Do, H.D. Do, A model for water adsorption in activated carbon, Carbon 38 (5) (2000) 767–773.
[8] J. Sung, Y.R. Shen, G.A. Waychunas, The interfacial structure of water/protonated alpha-Al_2O_3 (11(2)over-bar0) as a function of pH, J. Phys.-Cond. Matt. 24 (12) (2012).
[9] J. Sung, L. Zhang, C. Tian, Y.R. Shen, G.A. Waychunas, Effect of pH on the water/α-$Al_2O_3(1\bar{1}02)$ interface structure studied by sum-frequency vibrational spectroscopy, J. Phys. Chem. C 115 (28) (2011) 13887–13893.
[10] J. Sung, L. Zhang, C. Tian, G.A. Waychunas, Y.R. Shen, Surface structure of protonated R-sapphire (1102) studied by sum-frequency vibrational spectroscopy, J. Am. Chem. Soc. 133 (11) (2011) 3846–3853.
[11] J.F. Boily, Water structure and hydrogen bonding at goethite/water interfaces: implications for proton affinities, J. Phys. Chem. C 116 (7) (2012) 4714–4724.
[12] S.-Y. Ma, L.-M. Liu, S.-Q. Wang, Water film adsorbed on the α-Al_2O_3(0001) surface: structural properties and dynamical behaviors from first-principles molecular dynamics simulations, J. Phys. Chem. C 120 (10) (2016) 5398–5409.
[13] N.N. Casillas-Ituarte, H.C. Allen, Water, chloroform, acetonitrile, and atrazine adsorption to the amorphous silica surface studied by vibrational sum frequency generation spectroscopy, Chem. Phys. Lett. 483 (1–3) (2009) 884–898.
[14] P.J. Eng, T.P. Trainor, G.E. Brown, G.A. Waychunas, M. Newville, S.R. Sutton, M.L. Rivers, Structure of the hydrated alpha-Al_2O_3 (0001) surface, Science 288 (5468) (2000) 1029–1033.
[15] J.G. Catalano, Weak interfacial water ordering on isostructural hematite and corundum (001) surfaces, Geochim. Cosmochim. Acta 75 (8) (2011) 2062–2071.
[16] M.F.C. Andrade, H.Y. Ko, R. Car, A. Selloni, Structure, polarization, and sum frequency generation spectrum of interfacial water on anatase TiO_2, J. Phys. Chem. Lett. 9 (23) (2018) 6716–6721.
[17] A. Tuladhar, S.M. Piontek, E. Borguet, Insights on interfacial structure, dynamics, and proton transfer from ultrafast vibrational sum frequency generation spectroscopy of the alumina(0001)/water interface, J. Phys. Chem. C 121 (9) (2017) 5168–5177.
[18] Y. Nagata, T. Hasegawa, E.H.G. Backus, K. Usui, S. Yoshimune, T. Ohto, M. Bonn, The surface roughness, but not the water molecular orientation varies with temperature at the water–air interface, Phys. Chem. Chem. Phys. 17 (36) (2015) 23559–23564.
[19] J.D. Cyran, E.H.G. Backus, Y. Nagata, M. Bonn, Structure from dynamics: vibrational dynamics of interfacial water as a probe of aqueous heterogeneity, J. Phys. Chem. B 122 (14) (2018) 3667–3679.
[20] O. Björneholm, M.H. Hansen, A. Hodgson, L.-M. Liu, D.T. Limmer, A. Michaelides, P. Pedevilla, J. Rossmeisl, H. Shen, G. Tocci, E. Tyrode, M.-M. Walz, J. Werner, H. Bluhm, Water at Interfaces, Chem. Rev. 116 (13) (2016) 7698–7726.
[21] I.V. Stiopkin, C. Weeraman, P.A. Pieniazek, F.Y. Shalhout, J.L. Skinner, A.V. Benderskii, Hydrogen bonding at the water surface revealed by isotopic dilution spectroscopy, Nature 474 (7350) (2011) 192–195.
[22] M. Bonn, Y. Nagata, E.H.G. Backus, Molecular structure and dynamics of water at the water-air interface studied with surface-specific vibrational spectroscopy, Ang. Chem. Int. Ed. 54 (19) (2015) 5560–5576.
[23] C.D. Wick, I.F.W. Kuo, C.J. Mundy, L.X. Dang, The effect of polarizability for understanding the molecular structure of aqueous interfaces, J. Chem. Theo. Comp. 3 (6) (2007) 2002–2010.
[24] Q. Du, R. Superfine, E. Freysz, Y.R. Shen, Vibrational spectroscopy of water at the vapor/water interface, Phys. Rev. Lett. 70 (15) (1993) 2313–2316.
[25] W. Gan, D. Wu, Z. Zhang, R.R. Feng, H.F. Wang, Polarization and experimental configuration analyses of sum frequency generation vibrational spectra, structure, and orientational motion of the air/water interface, J. Chem. Phys. 124 (11) (2006) 114705.
[26] R.R. Feng, Y. Guo, H.F. Wang, Reorientation of the "free OH" group in the top-most layer of air/water interface of sodium fluoride aqueous solution probed with sum-frequency generation vibrational spectroscopy, J. Chem. Phys. 141 (18) (2014) 10.
[27] D. Verreault, W. Hua, H.C. Allen, From conventional to phase-sensitive vibrational sum frequency generation spectroscopy: probing water organization at aqueous interfaces, J. Phys. Chem. Lett. 3 (20) (2012) 3012–3028.
[28] J. Saavedra, T. Whittaker, Z. Chen, C.J. Pursell, R.M. Rioux, B.D. Chandler, Controlling activity and selectivity using water in the Au-catalysed preferential oxidation of CO in H_2, Nat. Chem. 8 (2016) 584.
[29] X. Song, J.F. Boily, Water vapor interactions with FeOOH particle surfaces, Chem. Phys. Lett. 560 (2013) 1–9.
[30] X. Song, J.F. Boily, Water vapor adsorption on goethite, Environ. Sci. Technol. 47 (13) (2013) 7171–7177.
[31] G.L. Richmond, Structure and bonding of molecules at aqueous surfaces, Ann. Rev. Phys. Chem. 52 (2001) 357–389.
[32] Y. Nagata, T. Ohto, E.H.G. Backus, M. Bonn, Molecular modeling of water interfaces: from molecular spectroscopy to thermodynamics, J. Phys. Chem. B 120 (16) (2016) 3785–3796.
[33] A.M. Jubb, W. Hua, H.C. Allen, Environmental Chemistry at Vapor/Water Interfaces: Insights from Vibrational Sum Frequency Generation Spectroscopy, in: M.A. Johnson, T.J. Martinez (Eds.), Annual Review of Physical Chemistry, Annual Reviews, Palo Alto, 2012, pp. 107–130.
[34] J. Schaefer, E.H.G. Backus, Y. Nagata, M. Bonn, Both inter- and intramolecular coupling of O-H groups determine the vibrational response of the water/air interface, J. Phys. Chem. Lett. 7 (22) (2016) 4591–4595.
[35] L. Zhang, C. Tian, G.A. Waychunas, Y.R. Shen, Structures and charging of alpha-alumina (0001)/water interfaces studied by sum-frequency vibrational spectroscopy, J. Am. Chem. Soc. 130 (24) (2008) 7686–7694.
[36] G. Ma, D. Liu, H.C. Allen, Piperidine adsorption on hydrated α-alumina (0001) surface studied by vibrational sum frequency generation spectroscopy, Langmuir 20 (26) (2004) 11620–11629.
[37] B. Braunschweig, S. Eissner, W. Daum, Molecular structure of a mineral/water interface: effects of surface nanoroughness of α-Al2O3 (0001), J. Phys. Chem. C 112 (6) (2008) 1751–1754.
[38] F.J. Tang, T. Ohto, T. Hasegawa, W.J. Xie, L.M. Xu, M. Bonn, Y. Nagata, Definition of free O-H groups of water at the air-water interface, J. Chem. Theo. Comp. 14 (1) (2018) 357–364.
[39] D.F. Bliss, Evolution and Application of the Kyropoulos Crystal Growth Method, in: R. Feigelson (Ed.), 50 Years of Progress in Crystal Growth, Elsevier, 2005.
[40] X. Song, J.F. Boily, Carbon dioxide binding at dry FeOOH mineral surfaces: evidence for structure-controlled speciation, Environ. Sci. Technol. 47 (16) (2013) 9241–9248.
[41] M.R. Conde, Properties of aqueous solutions of lithium and calcium chlorides: formulations for use in air conditioning equipment design, Int. J. Therm. Sci. 43 (2004) 367–382.
[42] H.F. Wang, W. Gan, R. Lu, Y. Rao, B.H. Wu, Quantitative spectral and orientational analysis in surface sum frequency generation vibrational spectroscopy (SFG-VS), Int. Rev. Phys. Chem. 24 (2) (2005) 191–256.
[43] X. Wei, Y.R. Shen, Motional effect in surface sum-frequency vibrational spectroscopy, Phys. Rev. Lett. 86 (21) (2001) 4799–4802.
[44] W. Gan, D. Wu, Z. Zhang, R.R. Feng, H.F. Wang, Polarization and experimental configuration analyses of sum frequency generation vibrational spectra, structure, and orientational motion of the air/water interface, J. Chem. Phys. 124 (11) (2006).
[45] X. Wei, S.C. Hong, X.W. Zhuang, T. Goto, Y.R. Shen, Nonlinear optical studies of liquid crystal alignment on a rubbed polyvinyl alcohol surface, Phys. Rev. E 62 (4) (2000) 5160–5172.
[46] S. Sun, F. Tang, S. Imoto, D.R. Moberg, T. Ohto, F. Paesani, M. Bonn, E.H.G. Backus, Y. Nagata, Orientational distribution of free O-H groups of interfacial water is exponential, Phys. Rev. Lett. 121 (24) (2018) 246101.
[47] W. Gan, R.R. Feng, H.F. Wang, Comment on orientational distributino of free O-H groups of interfacial water is exponential, Phys. Lett. Rev. (2019). in press.
[48] S. Sun, F. Tang, S. Imo, D.R. Moberg, T. Ohto, F. Paesani, M. Bonn, E.H.G. Backus, Y. Nagata, reply. Phys. Rev. Lett. Accepted (2019).
[49] J. Lutzenkirchen, T. Scharnweber, T. Ho, A. Striolo, M. Sulpizi, A. Abdelmonem, A set-up for simultaneous measurement of second harmonic generation and streaming potential and some test applications, J. Colloid Interface Sci. 529 (2018) 294–305.
[50] J. Lutzenkirchen, G.V. Franks, M. Plaschke, R. Zimmermann, F. Heberling, A. Abdelmonem, G.K. Darbha, D. Schild, A. Filby, P. Eng, J.G. Catalano, J. Rosenqvist, T. Preocanin, T. Aytug, D. Zhang, Y. Gan, B. Braunschweig, The surface chemistry of sapphire-c: a literature review and a study on various factors influencing its IEP, Adv. Colloid Interface Sci. 251 (2018) 1–25.
[51] R. Polly, B. Schimmelpfennig, M. Florsheimer, K. Kruse, A. AbdElMonem, R. Klenze, G. Rauhut, T. Fanghanel, Theoretical investigation of the water/corundum (0001) interface, J. Chem. Phys. 130 (6) (2009) 14.
[52] M. Pouvreau, J.A. Greathouse, R.T. Cygan, A.G. Kalinichev, Structure of hydrated gibbsite and brucite edge surfaces: DFT results and further development of the ClayFF classical force field with metal-O-H angle bending terms, J. Phys. Chem. C 121 (27) (2017) 14757–14771.
[53] L.W. Finger, R.M. Hazen, Crystal structure and isothermal compression of Fe_2O_3, Cr_2O_3 and V_2O_3 to 50 kbars, J. Appl. Phys. 51 (10) (1980) 5362–5367.
[54] D. van der Spoel, E. Lindahl, B. Hess, G. Groenhof, A.E. Mark, H.J.C. Berendsen, GROMACS: fast, flexible, and free, J. Comput. Chem. 26 (16) (2005) 1701–1718.
[55] R.T. Cygan, J.J. Liang, A.G. Kalinichev, Molecular models of hydroxide, oxyhydroxide, and clay phases and the development of a general force field, J. Phys. Chem. B 108 (4) (2004) 1255–1266.
[56] H.J.C. Berendsen, J.P. Postma, W.F. van Gunsterenand, J. Hermans, Interaction models for water in relation to protein hydration, in: Intermolecular Forces, D Reidel Publishing Company, 1981, pp. 331–342.

[57] H.J.C. Berendsen, J.P.M. Postma, W.F. Gunsterenand, J. Hermans, Intermolecular Forces, D. Riedel Publishing Company, Dordrecht, The Netherlands, 1981.
[58] R.W. Hockney, S.P. Goel, J.W. Eastwood, Quiet high-resolution computer models of a plasma, J. Comp. Phys. 14 (2) (1974) 148–158.
[59] S. Nose, M.L. Klein, Constant pressure molecular-dynamics for molecular-systems, Mol. Phys. 50 (5) (1983) 1055–1076.
[60] S. Miyamoto, P.A. Kollman, SETTLE - an analyical version of the shake and rattle algorithm for rigid water models, J. Comput. Chem. 13 (8) (1992) 952–962.
[61] B. Hess, H. Bekker, H.J.C. Berendsen, J. Fraaije, LINCS: a linear constraint solver for molecular simulations, J. Comput. Chem. 18 (12) (1997) 1463–1472.
[62] A. Luzar, D. Chandler, Hydrogen-bond kinetics in liquid water, Nature 379 (6560) (1996) 55–57.
[63] J. Teixeira, M.C. Bellissent-Funel, Dynamics of water studied by neutron scattering, J. Phys: Cond. Matt. 2 (S) (1990) SA105.
[64] A.K. Soper, M.G. Phillips, A new determination of the structure of water at 25°C, Chem. Phys. 107 (1) (1986) 47–60.
[65] G. Melani, Y. Nagata, J. Wirth, P. Saalfrank, Vibrational spectroscopy of hydroxylated alpha-Al2O3(0001) surfaces with and without water: an ab initio molecular dynamics study, J. Chem. Phys. 149 (1) (2018) 10.
[66] M. Flörsheimer, K. Kruse, R. Polly, A. Abdelmonem, B. Schimmelpfennig, R. Klenze, T. Fanghänel, Hydration of mineral surfaces probed at the molecular level, Langmuir 24 (23) (2008) 13434–13439.
[67] H. Knozinger, P. Ratnasamy, Catalytic aluminas - surface models and characterization of surface sites, Catal. Rev. - Sci. Eng. 17 (1) (1978) 31–70.
[68] G. Busca, The surface of transitional aluminas: a critical review, Catal. Today 226 (2014) 2–13.
[69] A. Boulesbaa, E. Borguet, Vibrational dynamics of interfacial water by free induction decay sum frequency generation (FID-SFG) at the Al_2O_3 (1120)/H2O interface, J. Phys. Chem. Lett. 5 (3) (2014) 528–533.
[70] X. Song, J.F. Boily, Water vapor diffusion into a nanostructured iron oxyhydroxide, Inorgan. Chem. 52 (12) (2013) 7107–7113.
[71] J.F. Boily, M. Yesilbas, M. Md Musleh Uddin, L. Baiqing, Y. Trushkina, G. Salazar-Alvarez, Thin water films at multifaceted hematite particle surfaces, Langmuir 31 (48) (2015) 13127–13137.
[72] P.B. Miranda, L. Xu, Y.R. Shen, M. Salmeron, Icelike water monolayer adsorbed on mica at room temperature, Phys. Rev. Lett. 81 (26) (1998) 5876.
[73] J. Zhou, E. Anim-Danso, Y. Zhang, Y. Zhou, A. Dhinojwala, Interfacial water at polyurethane-sapphire interface, Langmuir 31 (45) (2015) 12401–12407.
[74] I.F.W. Kuo, C.J. Mundy, B.L. Eggimann, M.J. McGrath, J.I. Siepmann, B. Chen, J. Vieceli, D.J. Tobias, Structure and dynamics of the aqueous liquid-vapor interface: a comprehensive particle-based simulation study, J. Phys. Chem. B 110 (8) (2006) 3738–3746.
[75] H. Wu, W.-K. Zhang, W. Gan, Z.-F. Cui, H.-F. Wang, Quantitative interpretation of polarization SFG vibrational spectra of air/methanol interface, Chinese J. Chem. Phys. 19 (3) (2006) 187–189.
[76] T.D. Kühne, T.A. Pascal, E. Kaxiras, Y. Jung, New insights into the structure of the vapor/water interface from large-scale first-principles simulations, J. Phys. Chem. Lett. 2 (2) (2011) 105–113.
[77] D.S. Walker, D.K. Hore, G.L. Richmond, Understandin the population, coordination, and orientation of water species contributing to the nonlinear optical spectroscopy of the vapor-water interface through molecular dynamics simulations, J. Phys. Chem. B. 110 (2006) 20451–20459.
[78] N.G. Petrik, P.L. Huestis, J.A. LaVerne, A.B. Aleksandrov, T.M. Orlando, G.A. Kimmel, Molecular water adsorption and reactions on alpha-Al_2O_3(0001) and alpha-alumina particles, J. Phys. Chem. C 122 (17) (2018) 9540–9551.